Structural basis for ligand binding modes of CTP synthase

Xian Zhou[1,†], Chen-Jun Guo[1,2,3,†], Chia-Chun Chang[1†], Jiale Zhong[1,2,3], Huan-Huan Hu[1,2,3], Guang-Ming Lu[1,2,3], and Ji-Long Liu[1*]

SUPPLEMENTAL INFORMATION

SUPPLEMENTAL TABLE S1 AND FIGURES S1-S12

SUPPLEMENTAL MOVIE S1

Table S1. Cryo-EM data collection and model refinement

	dmCTPS+Sub (EMD-30810, PDB 7DPT)	dmCTPS+Pro (EMD-30811, PDB 7DPW)
Data collection		
EM equipment	Titan Krios	Titan Krios
Detector	K3 camera	K3 camera
Magnification	22,500x	22,500x
Voltage (kV)	300	300
Electron exposure ((e–/Å^2))	60	60
Defocus range(μm)	-1.0 to -2.3	-1.0 to -2.3
Pixel size(Å)	0.53	0.53
Symmetry imposed	D2	D2
Number of collected movies	2878	2259
Initial particle images (no.)	424195	1563553
Final particle images (no.)	107556	344869
Map resolution (Å)	2.5	2.7
FSC threshold	0.143	0.143
Map resolution range (Å)	2.4 - 3.8	2.5 - 4.7
Refinement		
Initial model used (PDB code)	6L6Z	6LFG
Map sharpening B-factor(Å^2)	-77	-90
Model composition		
Non-hydrogen atoms	18036	17812
Protein residues	2224	2224
Ligands	UTP,ATP,GTP,DON	CTP
Waters	76	32
Ions	12	8
B factors(Å^2)		
Protein	97	68
Ligand	88	32
Water	87	38
R.m.s. deviations		
Bond lengths (Å)	0.006	0.008
Bond angles (°)	0.663	0.81
Validation		
MolProbity score	1.69	2.56
Clashscore	3.24	7.84
Poor rotamers (%)	1.44	8.02
Ramachandran plot		
Favored (%)	92.78	93.14
Allowed (%)	7.04	6.68
Disallowed (%)	0.18	0.18

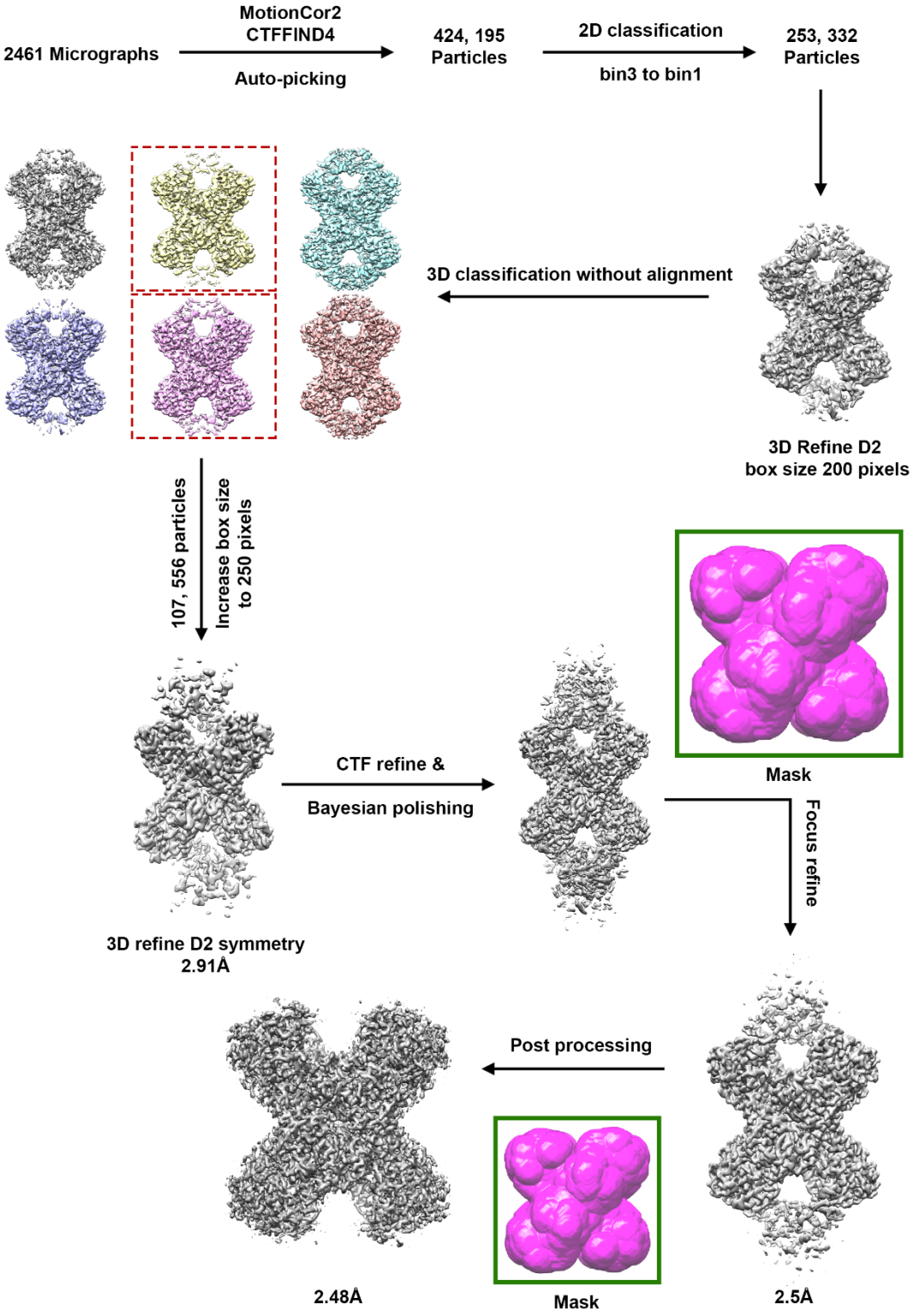

Figure S1. Image processing work flow of substrate-bound dmCTPS tetramer. In the reconstruction of the dmCTPS^{+Sub} tetramer, we collected 2461 micrographs and 253,332 particles were kept after 2D classification. After re-extraction of particles of dmCTPS^{+Sub} tetramer, different reconstructions were performed to generate the final map and model.

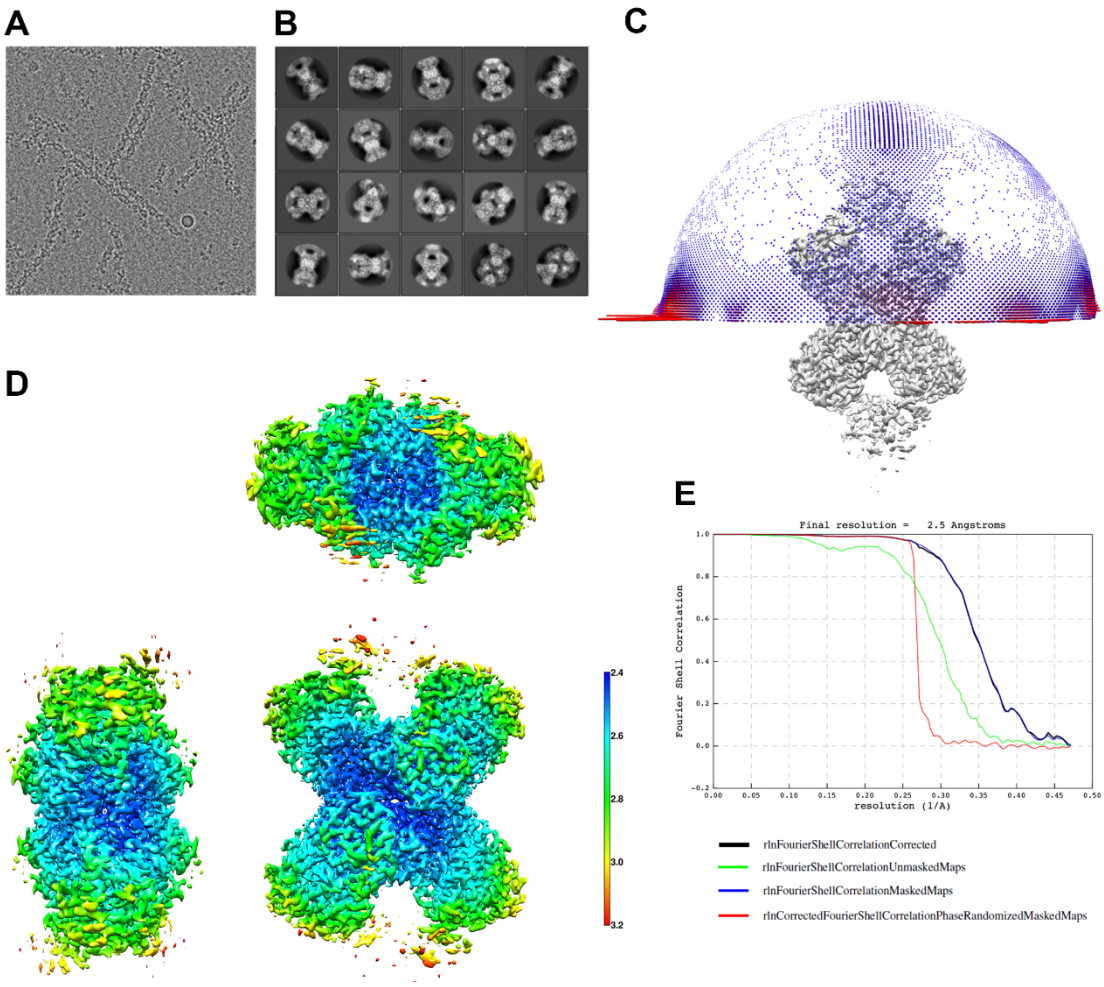

Figure S2. Statistics of the final density maps of the dmCTPS^{+Sub} tetramer. a, A representative cryo-EM micrograph of dmCTPS^{+Sub} tetramer/polymer. **b**, Representative 2D class averages of different views of the porcine dmCTPS^{+Sub} tetramer. **c**, Particle orientation distributions of the dmCTPS^{+Sub} tetramer in the last iteration of the 3D auto-refinement. **d**, Local resolution map of the dmCTPS^{+Sub} tetramer final 3D density map. **e**, Gold-standard FSC curve of the final density maps of the dmCTPS^{+Sub} tetramer.

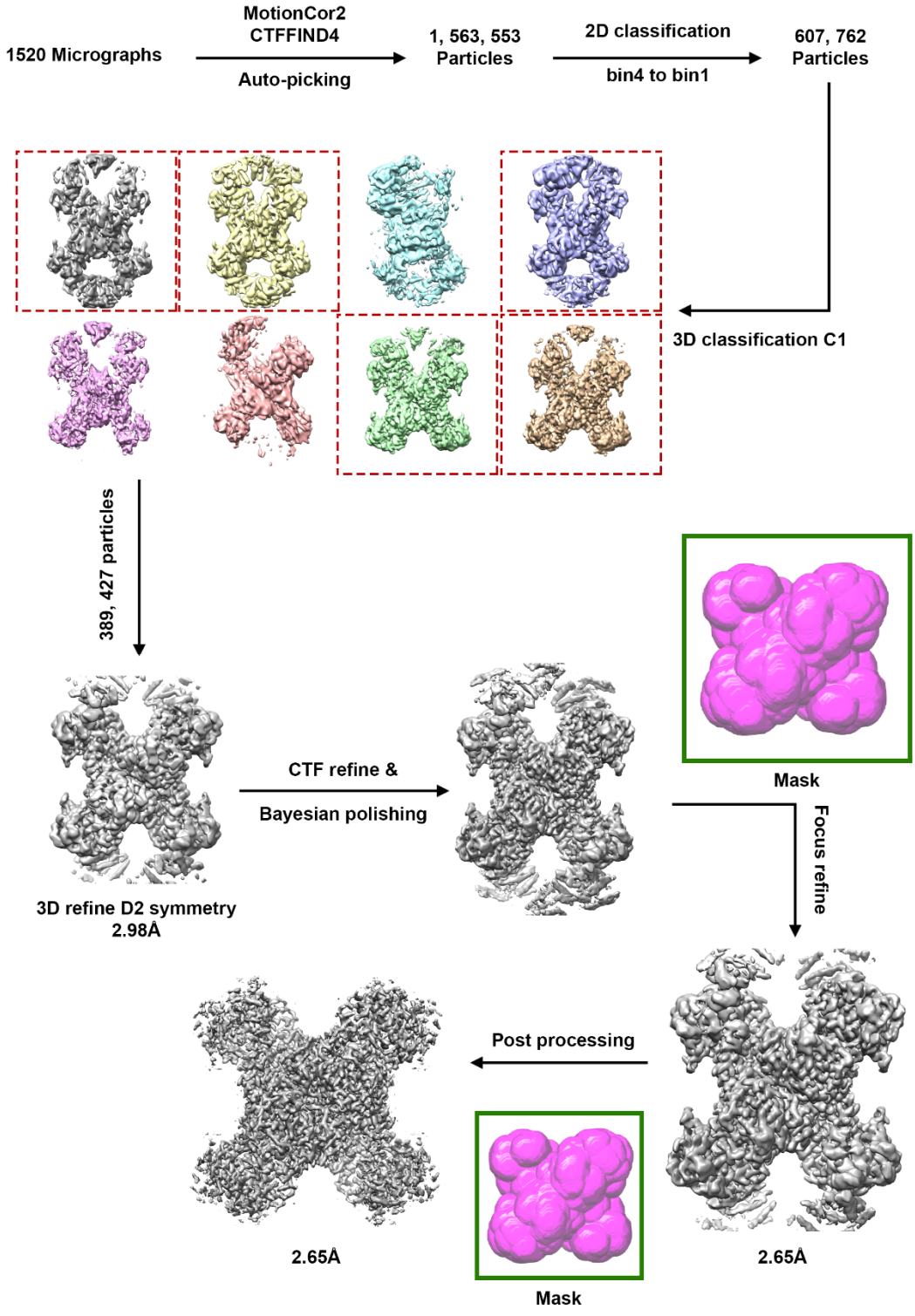

Figure S3. Image processing work flow of product-bound dmCTPS tetramer. In the reconstruction of the dmCTPS^{+Pro} tetramer, we collected 1520 micrographs and 607,762 particles were kept after 2D classification. After re-extraction of particles of dmCTPS^{+Pro} tetramer, different reconstructions were performed to generate the final map and model.

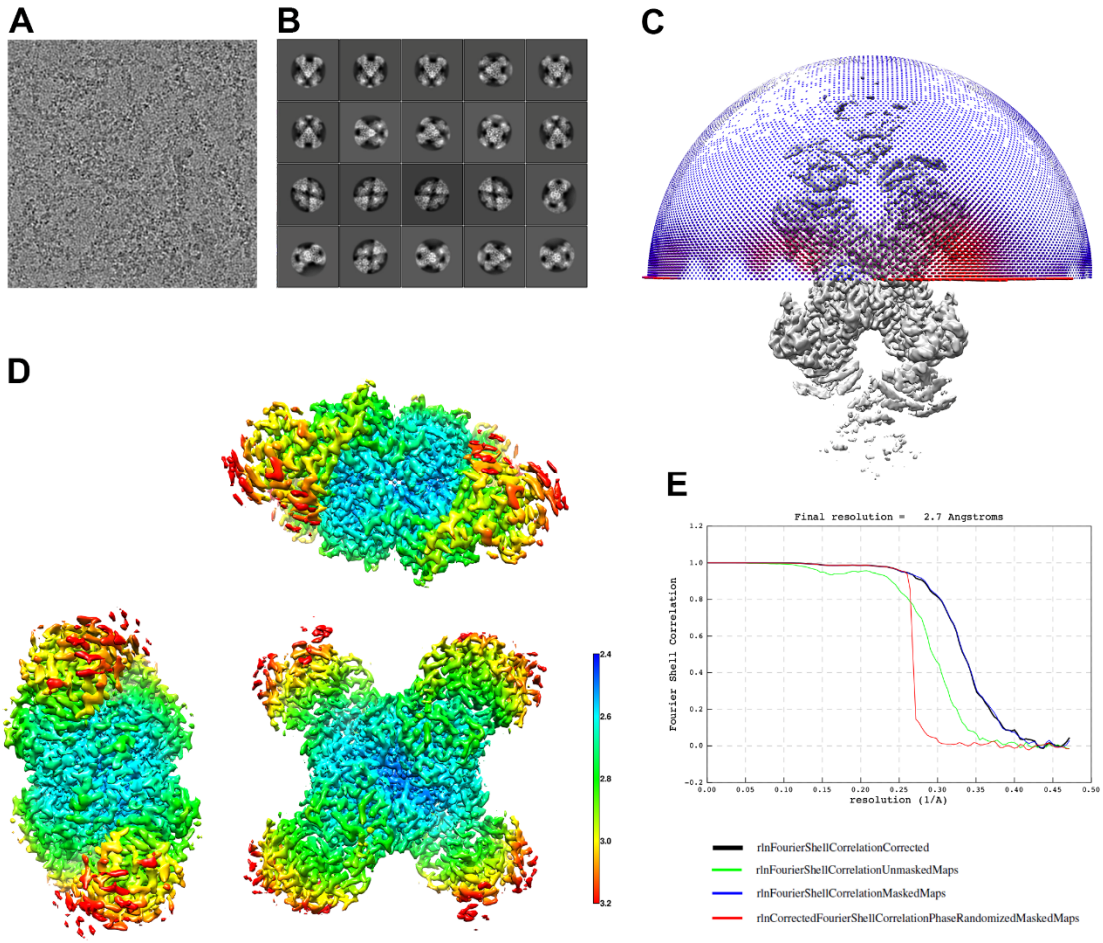

Figure S4. Statistics of the final density maps of the dmCTPS^{+Pro} tetramer. a, A representative cryo-EM micrograph of dmCTPS^{+Pro} tetramer/polymer. **b**, Representative 2D class averages of different views of the porcine dmCTPS^{+Pro} tetramer. **c**, Particle orientation distributions of the dmCTPS^{+Pro} tetramer in the last iteration of the 3D auto-refinement. **d**, Local resolution map of the dmCTPS^{+Pro} tetramer final 3D density map. **e**, Gold-standard FSC curve of the final density maps of the dmCTPS^{+Pro} tetramer.

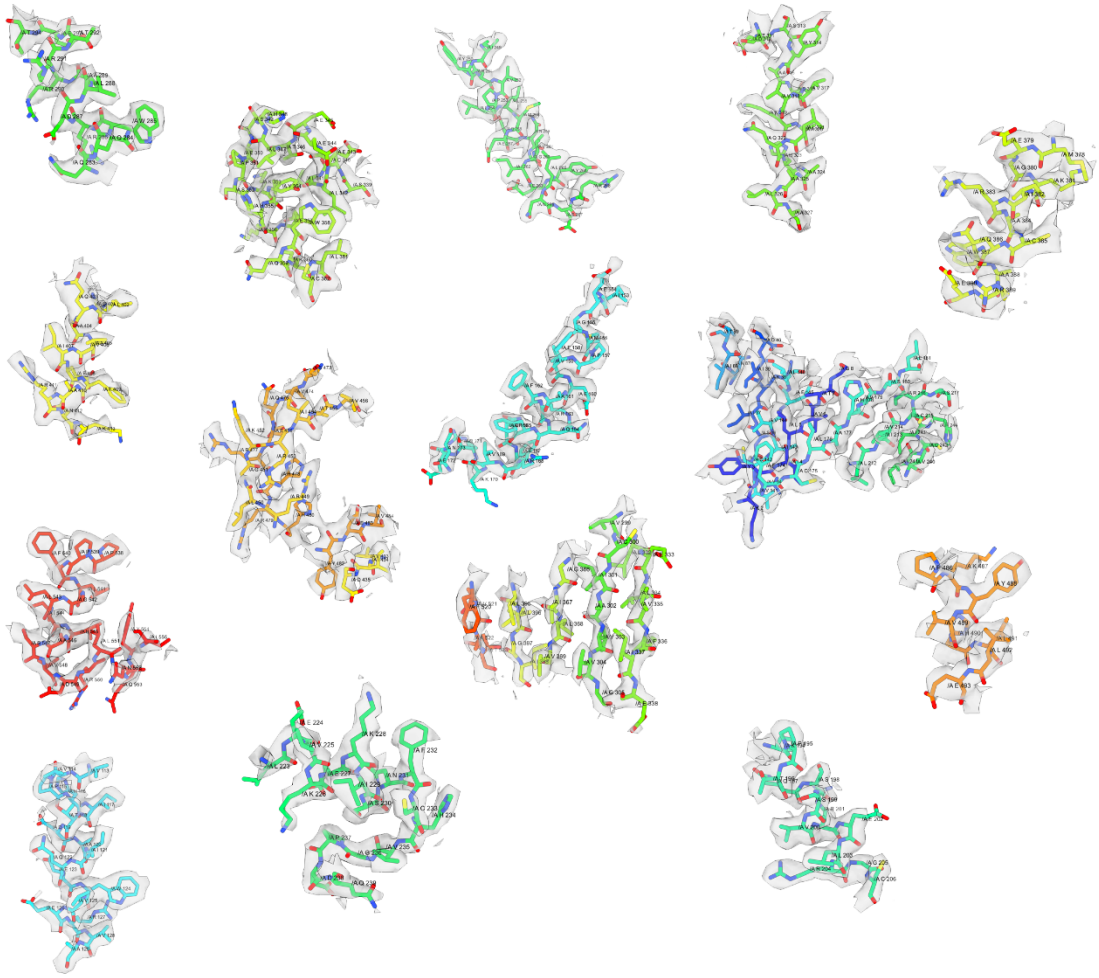

Figure S5. Representative electron density map of individual regions of dmCTPS^{+Sub} model.

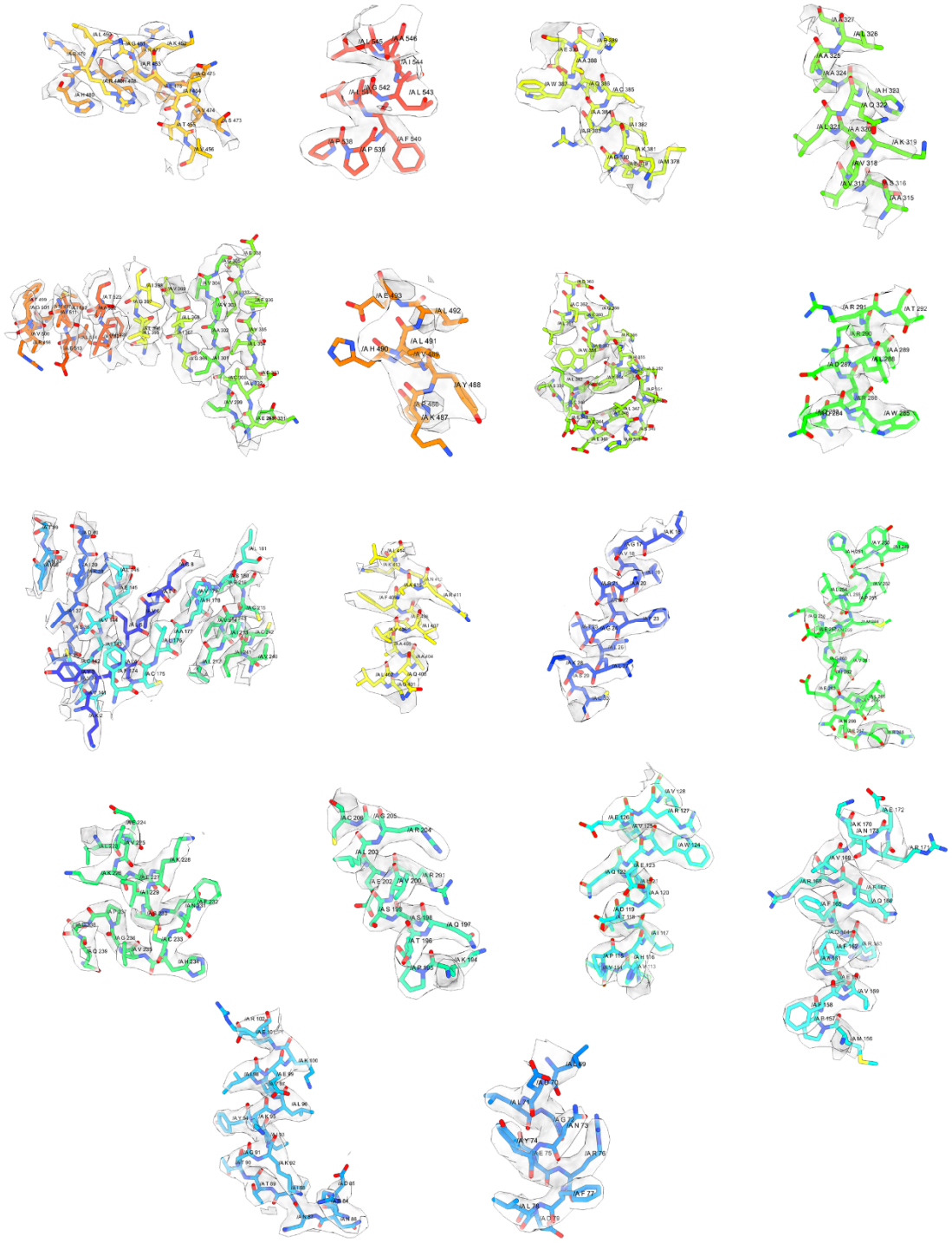

Figure S6. Representative electron density map of individual regions of dmCTPS^{+Pro} model.

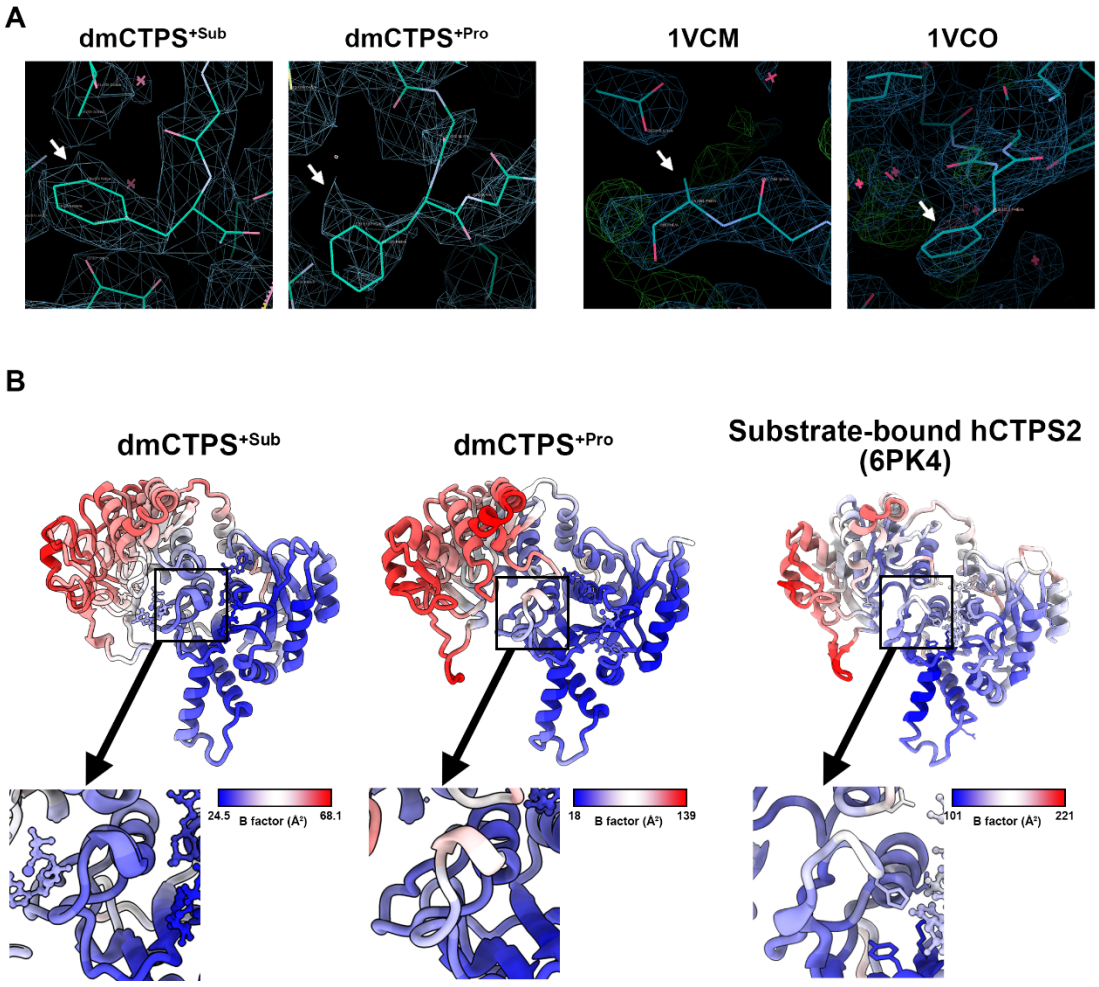

Figure S7. The comparisons of electron density maps of dmCTPS with reported CTPS models. a, The electron density maps of Phe373 in dmCTPS^{+Sub}, dmCTPS^{+Pro}, and of Phe365 in *Thermus thermophilus* CTPS in the apo state (1VCM) and the glutamine-bound state (1VCO). Phe373 in dmCTPS and Phe365 in ttCTPS are indicated by arrows. **b**, B factors are shown on monomers of dmCTPS^{+Sub}, dmCTPS^{+Pro} and substrate-bound hCTPS2 (6PK4) models. The region of the ammonia tunnel is highlighted.

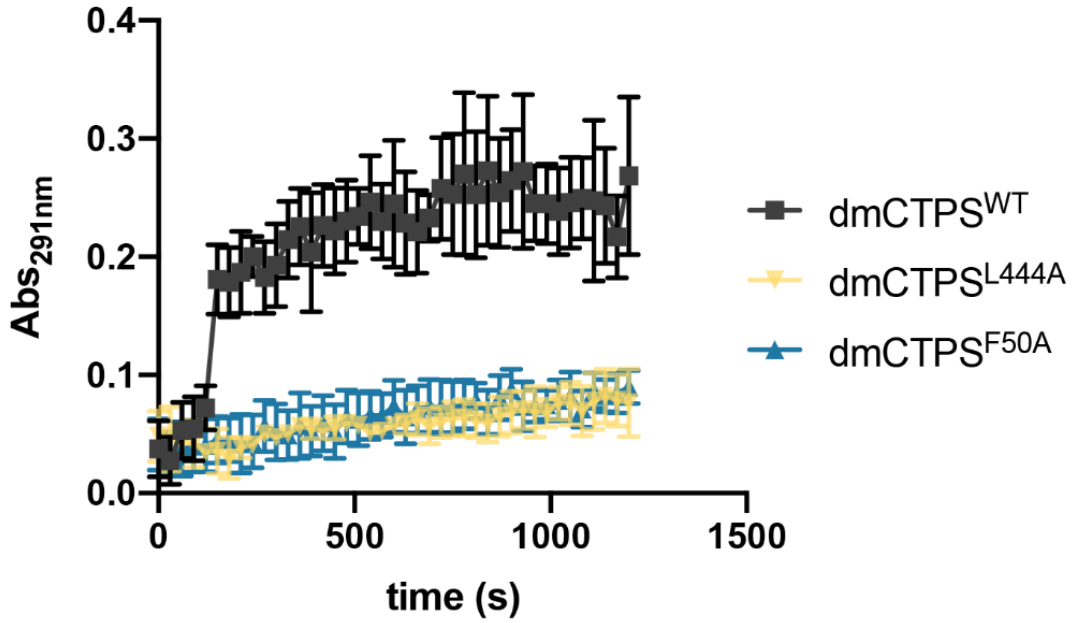

Figure S8. Analysis for generation of CTP by mutant dmCTPS (F50A and L444A) in condition with 2 mM of GTP.

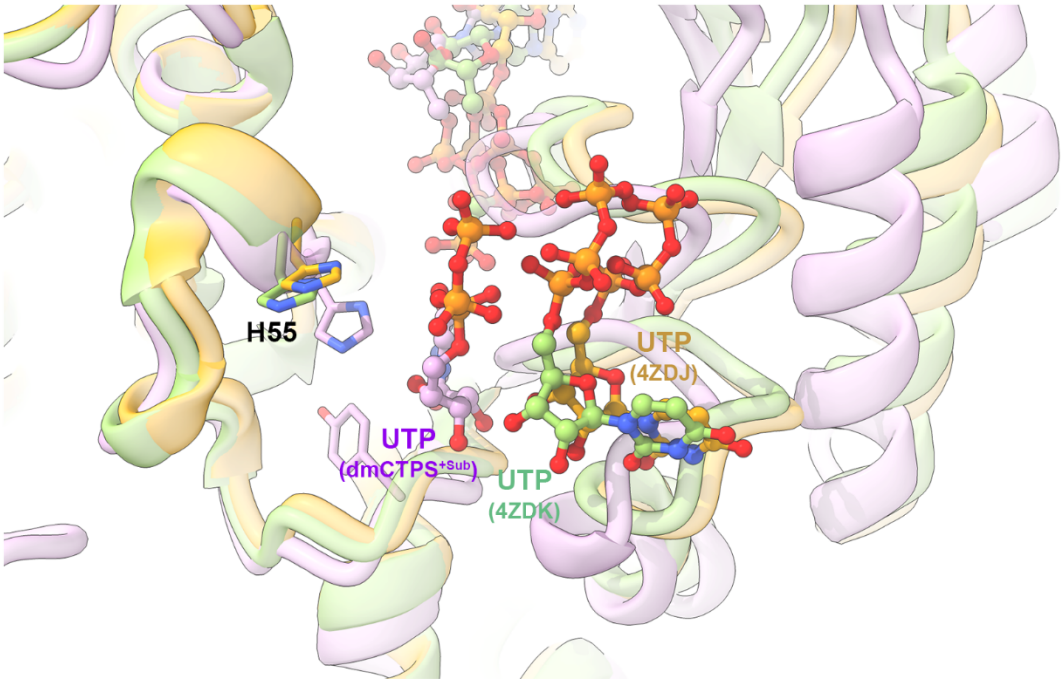

Figure S9. The structure comparison indicates the difference of distance between His55 and UTP in the open and closed CTPS conformations. The dmCTPS^{+Sub} model is shown in pink, the models of *Mycobacterium tuberculosis* CTPS (4ZDK, bound with UTP, ACP and DON) and (4ZDJ, bound with UTP) are shown in green and yellow, respectively.

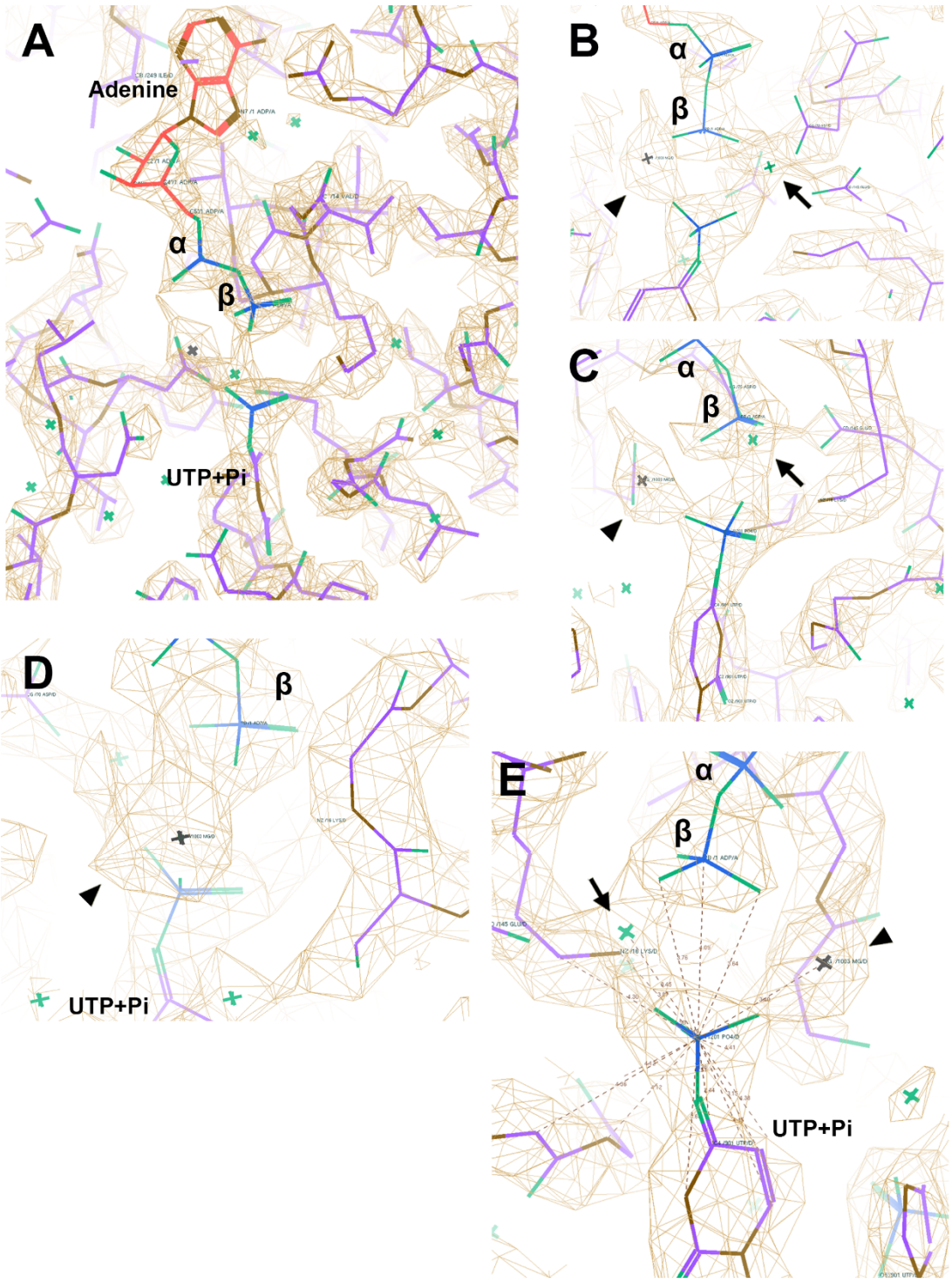

Figure S10. The electron density map of ligands at the AL domain active site of substrate-bound state. a, The general map of ligands at the AL domain when the map level was set as 10σ. In the map the α-phosphate and β-phosphate of the ATP match the density very well. However, the γ-phosphate of the ATP is not seen with the same setting. Meanwhile, a large density appears to be connected with the uracil of the UTP. **b**, **c**, There are two other density groups are located at both sides of the β-phosphate of ADP (indicated by arrow and arrowhead). Although the density indicated by the arrow

is connected with the β-phosphate, its size is too small to be a phosphate. In addition, it is also connected with Asp70, Glu145 and the additional density on the uracil, making it unlikely a phosphate. **d,** The density indicated by the arrowhead displays a density extension under lower map level (7.2σ), implying the presence of six bound water molecules. According to the catalytic process, we suggest the additional density on the uracil is the γ-phosphate of the ATP transferred to the 4-oxygen atom of the uracil base and the arrow and arrowhead indicate a water and a Mg^{2+} ion, respectively. **e,** The distance from the β-phosphate of ADP to the phosphate on the uracil is about 4.09 Å, far larger than the ordinary distance between β- and γ-phosphate. Meanwhile, the Mg^{2+} is slightly merged with the phosphate on the uracil. These suggest that transfer of γ-phosphate which is catalyzed by the Mg^{2+} is captured in our model.

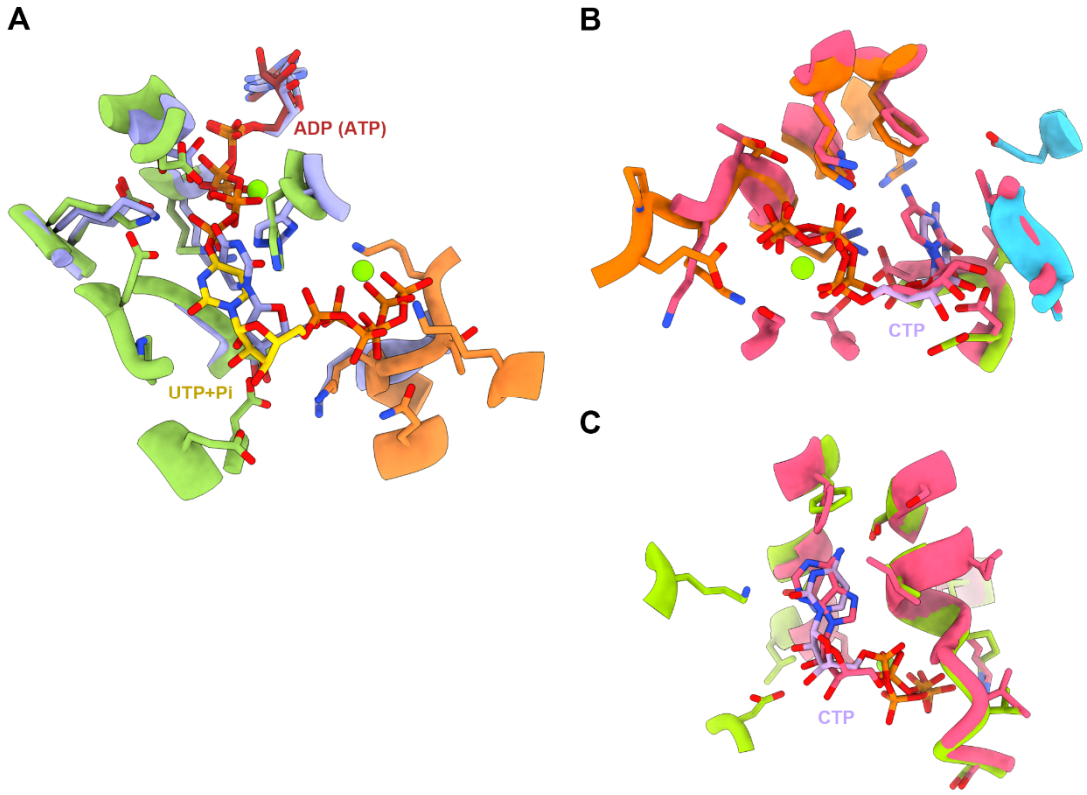

Figure S11. The comparison of dmCTPS and hCTPS2 at ATP/ADP, UTP and CTP binding sites. a, The structural comparison of dmCTPS^{+Sub} and substrate-bound hCTPS2 (6PK4) shows similar binding modes of ATP/ADP and UTP. **b** and **c**, The structural comparison of dmCTPS^{+Pro} and product-bound hCTPS2 (6PK7) shows the binding modes of CTP at UTP binding site (**b**) and ADP binding site (**c**).

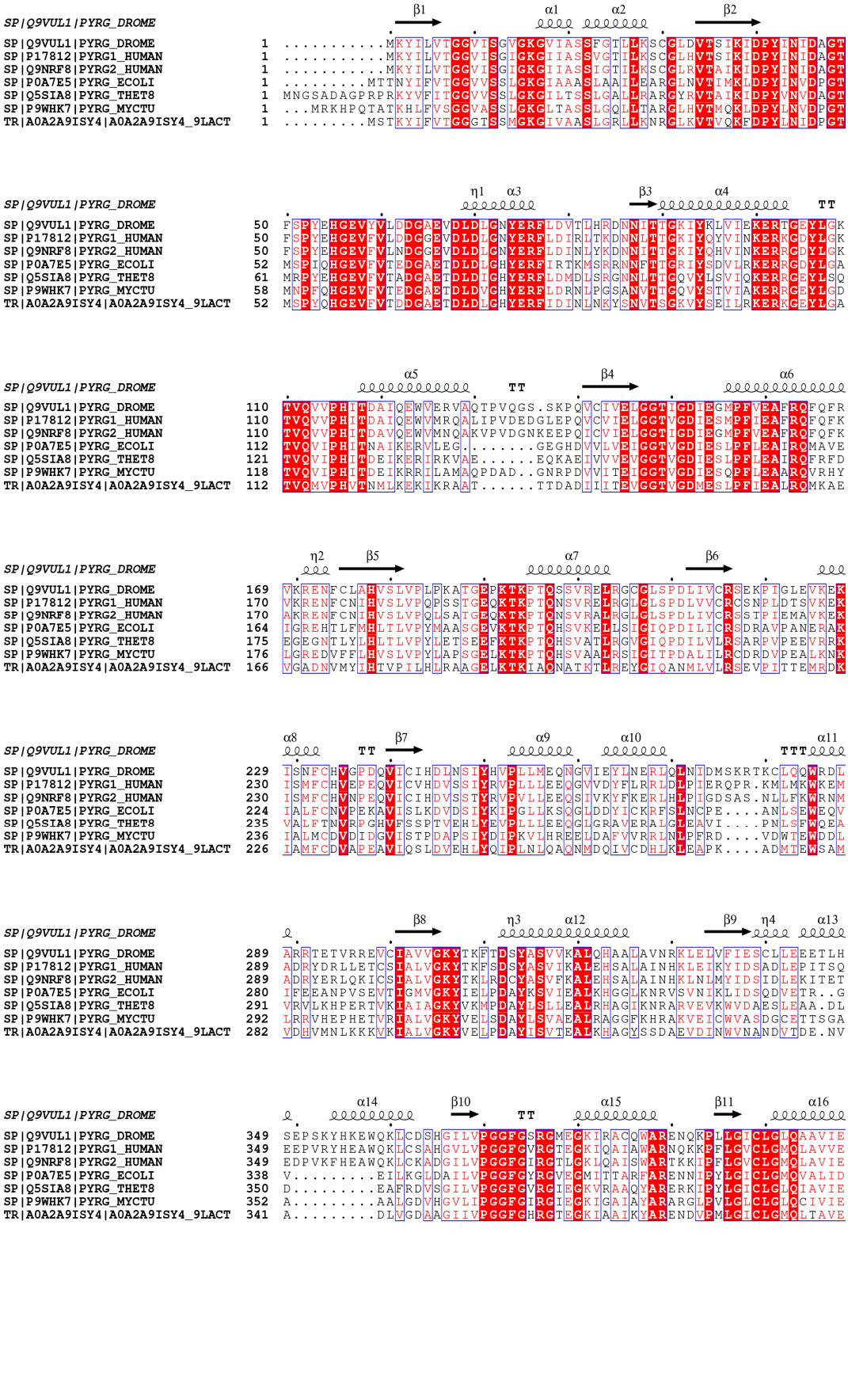
SP|Q9VUL1|PYRG_DROME
SP|Q9VUL1|PYRG_DROME 1
SP|P17812|PYRG1_HUMAN 1
SP|Q9NRF8|PYRG2_HUMAN 1
SP|P0A7E5|PYRG_ECOLI 1
SP|Q5SIA8|PYRG_THET8 1
SP|P9WHK7|PYRG_MYCTU 1
TR|A0A2A9ISY4|A0A2A9ISY4_9LACT 1
SP|Q9VUL1|PYRG_DROME 50
SP|P17812|PYRG1_HUMAN 50
SP|Q9NRF8|PYRG2_HUMAN 50
SP|P0A7E5|PYRG_ECOLI 52
SP|Q5SIA8|PYRG_THET8 61
SP|P9WHK7|PYRG_MYCTU 58
TR|A0A2A9ISY4|A0A2A9ISY4_9LACT 52
SP|Q9VUL1|PYRG_DROME 110
SP|P17812|PYRG1_HUMAN 110
SP|Q9NRF8|PYRG2_HUMAN 110
SP|P0A7E5|PYRG_ECOLI 112
SP|Q5SIA8|PYRG_THET8 121
SP|P9WHK7|PYRG_MYCTU 118
TR|A0A2A9ISY4|A0A2A9ISY4_9LACT 112
SP|Q9VUL1|PYRG_DROME 169
SP|P17812|PYRG1_HUMAN 170
SP|Q9NRF8|PYRG2_HUMAN 170
SP|P0A7E5|PYRG_ECOLI 164
SP|Q5SIA8|PYRG_THET8 175
SP|P9WHK7|PYRG_MYCTU 176
TR|A0A2A9ISY4|A0A2A9ISY4_9LACT 166
SP|Q9VUL1|PYRG_DROME 229
SP|P17812|PYRG1_HUMAN 230
SP|Q9NRF8|PYRG2_HUMAN 230
SP|P0A7E5|PYRG_ECOLI 224
SP|Q5SIA8|PYRG_THET8 235
SP|P9WHK7|PYRG_MYCTU 236
TR|A0A2A9ISY4|A0A2A9ISY4_9LACT 226
SP|Q9VUL1|PYRG_DROME 289
SP|P17812|PYRG1_HUMAN 289
SP|Q9NRF8|PYRG2_HUMAN 289
SP|P0A7E5|PYRG_ECOLI 280
SP|Q5SIA8|PYRG_THET8 291
SP|P9WHK7|PYRG_MYCTU 292
TR|A0A2A9ISY4|A0A2A9ISY4_9LACT 282
SP|Q9VUL1|PYRG_DROME 349
SP|P17812|PYRG1_HUMAN 349
SP|Q9NRF8|PYRG2_HUMAN 349
SP|P0A7E5|PYRG_ECOLI 338
SP|Q5SIA8|PYRG_THET8 350
SP|P9WHK7|PYRG_MYCTU 352
TR|A0A2A9ISY4|A0A2A9ISY4_9LACT 341

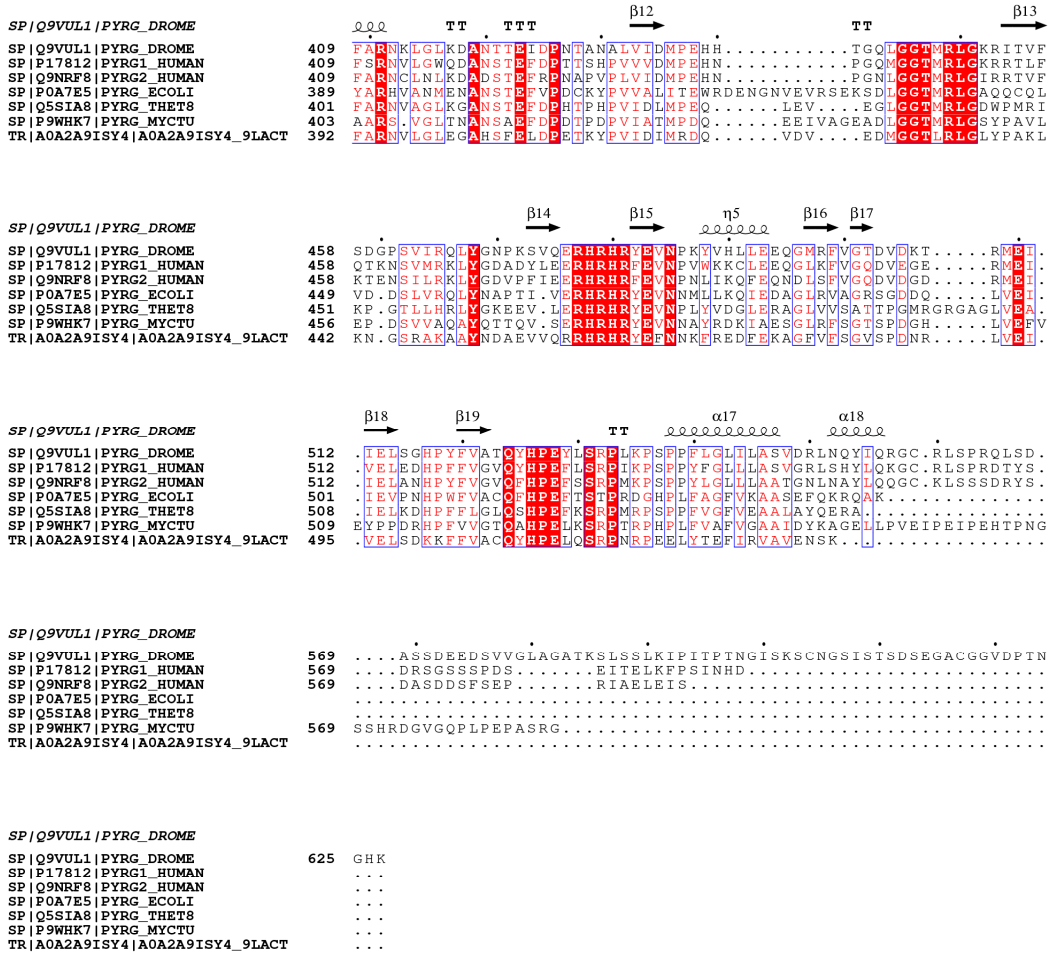

Figure S12. Comparison of CTPS sequences of various organisms.

Legends for SI Appendix videos

SUPPLEMENTAL MOVIE S1. Animation of CTPS morphing from the CTP-state to DON-state tetramer conformations. The movie displays the dmCTPS structure morphed from product-bound to substrate-bound state. Colored by monomer.